Adaptive Motion Planning via Dynamic Constraints Satisfaction for for Autonomous Mobile Robots

Appendix

Constraint Satisfaction Modeling

We formulate the functions to evaluate the constraint satisfaction in the paper. Here, we classified the relaxable constraints into three categories ($\mathrm{DS}^1(\mathcal{X}_i)$, $\mathrm{DS}^2(\mathcal{X}_i)$, $\mathrm{DS}^3(\mathcal{X}_i)$) based on their relationship with target values, i.e., LESS THAN, MORE THAN and AS CLOSE AS POSSIBLE. Correspondingly, the functions to evaluate constraint satisfaction, and the detailed fuzzy membership functions for $\mathrm{DS}^1(\mathcal{X}_i)$, $\mathrm{DS}^2(\mathcal{X}_i)$, and $\mathrm{DS}^2(\mathcal{X}_i)$ are listed as follows:

$$\mathrm{DS}^1(\mathcal{X}_i) = \begin{cases} \frac{ub_i - \mathcal{X}_i}{ub_i - g_i} & g_i < \mathcal{X}_i \leq ub_i \\ 1 & \mathcal{X}_i \leq g_i \\ 0 & otherwise \end{cases}$$

$$\mathrm{DS}^2(\mathcal{X}_i) = \begin{cases} \frac{\mathcal{X}_i - lb_i}{g_i - lb_i} & lb_i \leq \mathcal{X}_i < g_i \\ 1 & \mathcal{X}_i \geq g_i \\ 0 & otherwise \end{cases}$$

$$\mathrm{DS}^3(\mathcal{X}_i) = \begin{cases} \frac{\mathcal{X}_i - lb_i}{g_{i,1}} & lb_i \leq \mathcal{X}_i < g_{i,1} \\ 1 & g_{i,1} \leq \mathcal{X}_i \leq g_{i,2} \\ \frac{ub_i - \mathcal{X}_i}{ub_i - g_i} & g_{i,2} < \mathcal{X}_i \leq ub_i \\ 0 & otherwise \end{cases}$$

$$\mathrm{DS}^0(\mathcal{X}_i) = \begin{cases} 1, & \text{if } \mathcal{X}_i \text{ satisfy } \mathcal{C}_{nr,i} \\ 0, & \text{otherwise} \end{cases}$$

- Safety: The indicator to evaluate the safety constraint is the collision risk of UAV during the flight. Supposing that the obstacles detected by the UAV at time instant k is $\mathcal{O}_k$, while the current state of UAV is s_k. Thus, the QM of safety is $\mathcal{X}_{S_{o,k}} = \frac{\|\boldsymbol{x}_k - \boldsymbol{x}_o\|_2 - r_a - r_o}{D_o}, \forall o \in \mathcal{O}_k$. Such that the average distance between UAV and the center of obstacle reflects the safety risk.

$$\mathrm{DS}^2(\mathcal{X}_{S_{o,k}}) = \begin{cases} 1, & \mathcal{X}_{S_{o,k}} \geq 1 \\ 0, & \mathcal{X}_{S_{o,k}} < 0 \\ \mathcal{X}_{S_{o,k}}, & otherwise \end{cases}$$

- Privacy: Based on the privacy risk model illustrated in (Luo et al. 2020), the privacy risk is affected by the distance between the UAV and private regions, as well as the working state of sensors. The QM of privacy at time instant k is defined as $\mathcal{X}_{P_c,k} = 1 - \|\boldsymbol{\omega}_k\| \frac{(r_a + r_c + D_c) - \|\boldsymbol{x}_k - \boldsymbol{x}_c\|_2}{D_c}, \forall c \in \mathcal{C}_k$. We have the satisfaction function using the formulation of DS^2:

$$\mathrm{DS}^2(\mathcal{X}_{P_c,k}) = \begin{cases} 1, & \mathcal{X}_{P_c,k} \geq 1, \\ 0, & \|\boldsymbol{x}_k - \boldsymbol{x}_c\|_2 < r_a + r_c, \\ \mathcal{X}_{P_c,k}, & \text{otherwise} \end{cases}$$

- Timelines: The total traveling time from time instant i to j is denoted as $\xi_{ij} = \sum_{k=i}^{j-1} \frac{\|\boldsymbol{x}_{k+1} - \boldsymbol{x}_k\|_2}{\boldsymbol{v}_k}$. The indicator of timeliness is $\mathcal{X}_\xi = \xi_{0T}$, the degree of satisfaction of the timeliness constraint of the whole trajectory DS_ξ is:

$$\mathrm{DS}^1(\mathcal{X}_\xi) = \begin{cases} 1, & \mathcal{X}_\xi \leq \Delta_t \\ \dfrac{\Delta - \mathcal{X}_\xi}{\Delta - \Delta_t}, & \Delta_t < \mathcal{X}_\xi \leq \Delta \\ 0, & \mathcal{X}_\xi > \Delta \end{cases}$$

- Accuracy: The average quality of the information collected during the mission is denoted as $\mathcal{X}_\varphi = \frac{1}{\xi_{0T}} \sum_{k=0}^{T-1} \|\boldsymbol{w}\| \tau$, the degree of satisfaction is DS_φ is:

$$\mathrm{DS}^2(\mathcal{X}_\varphi) = \begin{cases} 1, & \mathcal{X}_\varphi \geq A_t \\ \dfrac{\mathcal{X}_\varphi - A}{A_t - A}, & A \leq \mathcal{X}_\varphi < A_t \\ 0, & \mathcal{X}_\varphi < A \end{cases}$$

- Energy-saving: The total energy consumption from time instant i to j is denoted as $e_{ij} = \sum_{k=i}^{j-1} \|\boldsymbol{x}_{k+1} - \boldsymbol{x}_k\|_2 + \eta_1 \cdot \|\boldsymbol{v}_{k+1} - \boldsymbol{v}_k\|_2 + \eta_2 \cdot \|\boldsymbol{w}_k\| \tau$. The indicator of energy consumption is $\mathcal{X}_E = e_{0T}$, the degree of satisfaction of energy constraint DS_E is:

$$\mathrm{DS}^1(\mathcal{X}_E) = \begin{cases} 1, & \mathcal{X}_E \leq E_t \\ \dfrac{E - \mathcal{X}_e}{E - E_t}, & E_t < \mathcal{X}_e \leq E \\ 0, & \mathcal{X}_E > E \end{cases}$$

Experiment Results

We show the details of the experimental results in the UAV prototype discussed in the paper.

Table 1: constraints-driven adaptation results for different scales of environment

Scale		*Accuracy* [%]	*Traveling Time* [s]	*Energy Consumption* [unit]	*Safety*	*Privacy*	*Real-time Performance*
50	$\mathcal{C}_r$	A_t=90	Δ_t=60	E_t=100	D_o=5m	D_p=10m	Adaptation Rate
	$\mathcal{C}_{nr}$	A=80	Δ=90	E=150	r_o=5m	r_p=5m	6/120
	$\mathcal{X}$	90	60.00	105.57	0	0	Overhead
	$\mathcal{DS}$	100%	100%	88.85%	100%	100%	Avg. 0.066s Std. 0.139s
100	$\mathcal{C}_r$	A_t=90	Δ_t=90	E_t=200	D_o=5m	D_p=10m	Adaptation Rate
	$\mathcal{C}_{nr}$	A=80	Δ=150	E=300	r_o=5m	r_p=5m	3/203
	$\mathcal{X}$	90	101.50	210.94	0	0.1534	Overhead
	$\mathcal{DS}$	100%	80.83%	89.06%	100%	99.98%	Avg. 0.132s Std. 0.180s

Scalability To demonstrate the scalability of ACMP with respect to different environments, we further simulated the UAV case on two selected real urban environments from the open building dataset of Portland in USA (Burian et al. 2002). We used ArcGIS map to set up a 3D model based on the method in (Hidalgo-Panagua et al. 2017). Their original spaces are $500 \times 500 \times 100m^3$ and $10^3 \times 10^3 \times 100\ m^3$, and compressed into $50 \times 50 \times 10\ m^3$ and $100 \times 100 \times 10\ m^3$, respectively. In the dataset, we can also obtain the longitude and latitude of the center of each building, as well as its average height and building types (i.e., industrial and commercial buildings, houses and apartments for living). The buildings for industrial and commercial use are viewed as obstacles, while houses and apartments are viewed as private regions. We used ArcGIS map to set up a 3D model according to the method introduced in (Hidalgo-Panagua et al. 2017). As shown in Fig. 2, the process of real urban scenarios modeling is explained. We set the range of longitude and latitude of working space on the ArcGIS map, and all the building are marked as blue (Fig. 2(a)). Then the ArcGIS map is turned into a binary map. Thus a 3D model of the urban scene is set up with the scale of $500m \times 500m \times 100m$ in Fig. 2(c).

In each case, the flight task of UAV is to travel from the position $[0, 0, 0]$ to the destination $[49, 49, 0]$ and $[99, 99, 0]$ respectively, within the budget of accuracy, time and energy, as well as minor safety and privacy risk. The trajectory, state transition and constraint achievement of the UAV at each time instant are shown in Figure 2(d), Figure 2(e) and Figure 2(f). So as to the scale of $1000m \times 1000m \times 100m$ in Figure 3. Table 1 summarizes the constraint adaptation results in these two settings. we find that the states generated from ACMP and the PD controller are almost the same, indicating that the planning results of ACMP can be translated by the PD controller and executed by the UAV effectively.

From our simulation results, in Setting 2, the flight task is completed in 60.07 s, consuming 106.27 units of energy without safety and privacy risk. In Setting 3, the task is finished in 101.5 s, consuming 210.94 units of energy. It does not have safety risk, but gets 4 points along the trajectory where the soft goal of privacy-preserving is violated. This results in an average 99.98% constraints satisfaction along the path. ACMP has high scalability as the two important steps *Constraints Satisfaction Checking* and *Constraints Satisfaction Optimization* are solved by SQP, which can handle large-scale optimization problems. In contrast, SCMP fails to compute a motion plan at real-time when the size of workspace increases.

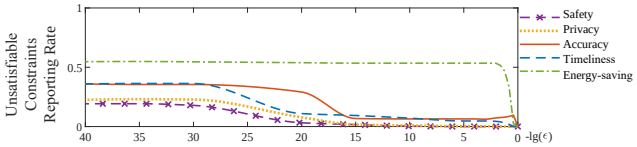

Figure 1: Unsatisfiable constraints reporting rate. (UAV case, $\rho_o = 2\%, \rho_p = 2\%$)

Choice of violation tolerance Given a violation tolerance, the average rate of time instants violating soft goals is recorded per simulation, as shown in Fig. 1. We choose $\epsilon_{SR,PR,\varphi,\xi,e} = \{10^{-20}, 10^{-20}, 10^{-10}, 10^{-20}, 0.005\}$ for the UAV case, the average rates of time instants that do not report violation of the soft goals of safety, privacy, timeliness, accuracy, and energy-saving in the UAV scenario are 16.0%, 14.7%, 29.0%, 25.5%, and 1.1% respectively. These results show that choosing the right violation tolerance parameters can help determine the appropriate set of unsatisfied constraints with a smaller impact on the algorithm's efficiency. In the case where the choice of tolerance parameter may affect the convergence in the *constraints Satisfaction Optimization* step and result in no feasible solutions, ACMP can directly leverage the planning results from the *constraints Satisfaction Checking* step, as illustrated in lines 13 and 14 in Algorithm 1.

UUV Oceanic Surveillance

This example originates from (Shevtsov and Weyns 2016; Shevtsov, Weyns, and Maggio 2019). Rather than considering single-objective optimization for the UUV scenario in (Shevtsov and Weyns 2016; Shevtsov, Weyns, and Maggio 2019), we extended it to achieve multiple dynamic constraints under uncertainties and disturbances through ACMP, while other configurations like sensors are kept the same as (Shevtsov and Weyns 2016). The constraints to achieve in this scenario are listed as follows:

- Scanning Distance (C_l): A segment of surface over a distance of $L_t = 100$ km is expected to be examined by

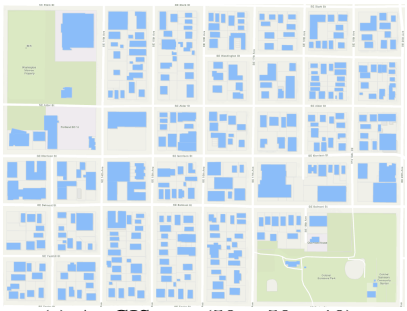

(a) ArcGIS map ($50 \times 50 \times 10$).

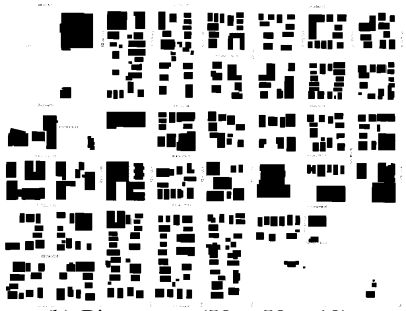

(b) Binary map ($50 \times 50 \times 10$).

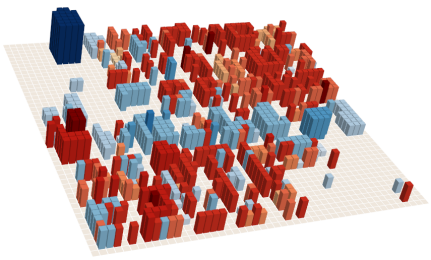

(c) Grid map ($50 \times 50 \times 10$).

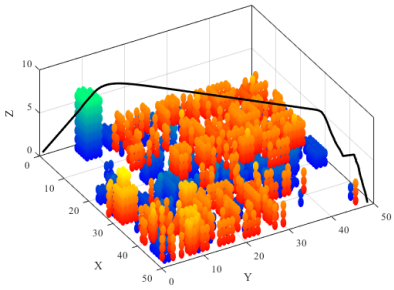

(d) Flight Trajectory of UAV.

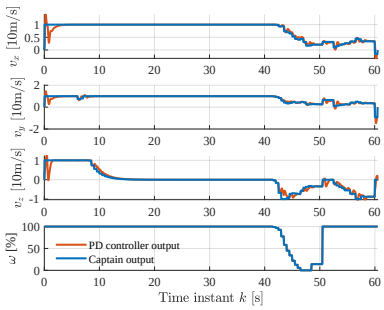

(e) State of UAV during the flight.

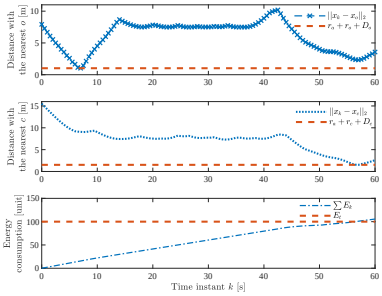

(f) Constraint Satisfaction of UAV during the flight.

Figure 2: Environment modeling with the scale of $500m \times 500m \times 100m$.

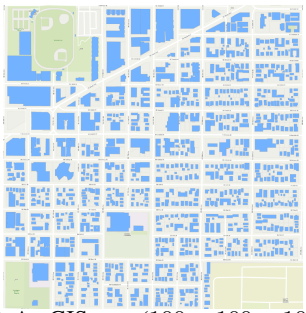

(a) ArcGIS map ($100 \times 100 \times 10$).

(b) Binary map ($100 \times 100 \times 10$).

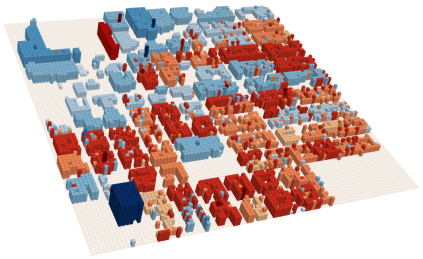

(c) Grid map ($100 \times 100 \times 10$).

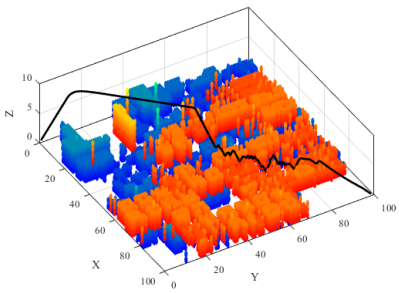

(d) Flight Trajectory of UAV.

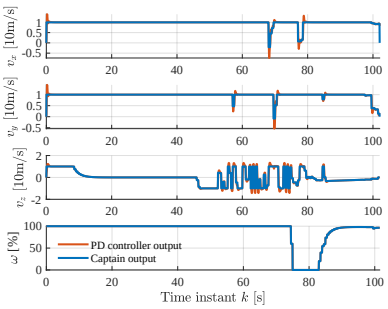

(e) State of UAV during the flight.

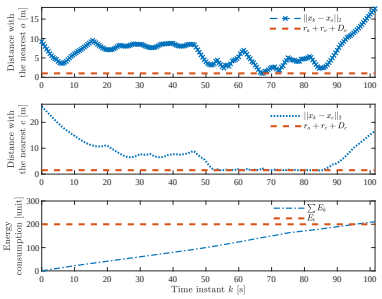

(f) Constraint satisfaction of UAV during the flight.

Figure 3: Environment modeling with the scale of $1000m \times 1000m \times 100m$.

the UUV within $\Delta = 10$ hours, while the threshold of surveillance distance is $L = 90$ km.

- Energy Consumption (C_E): A total amount of energy $E_t = 5.4$ MJ is expected to be consumed, while the maximum amount of energy is $E = 6$ MJ.
- Accuracy (C_φ): The accuracy of sensor measurements is targeted at $A_t = 90\%$, while the accuracy threshold is set as $A = 80\%$.

Constraints Satisfaction Modeling

The UUV is equipped with 5 sensors for ocean surveillance. The scanning time 10 hours is 360 time instance, $x_i, i \in [1, 5]$ is the portion of time the sensor i should be used during system operation in each instance. Acc_i is the accuracy of sensor i; E_i is the energy consumed by sensor; V_i is the scanning speed of sensor. q_i is portion of accuracy of sensor and p_i is for scanning speed respectively in decimals. The energy consumed is related with working accuracy and speed of sensor. The corresponding measures are listed as follows: $\mathcal{X}_l = \sum_{k=0}^{T}\sum_{i=0}^{N} x_i q_i V_i \tau$, $\mathcal{X}_E = \sum_{k=0}^{T}\sum_{i=0}^{N} x_i E_i \cdot \frac{e^{p_i+q_i}-1}{e^2-1}\tau$, and $\mathcal{X}_\varphi = \sum_{k=0}^{T}\sum_{i=0}^{N} x_i p_i Acc_i$, where $T = 360$, i.e., adaptations is performed every 100 surface measurements of the UUV state,, and the time instance k incremented by $1 \sim 100$. The constraint satisfaction functions are listed as follows:

- Scanning distance: A segment of surface over a distance of $L_t = 100$ km is expected to be examined by the UUV within $\Delta = 10$ hours, while the distance threshold is $L = 90$ km.

$$\mathrm{DS}^2(\mathcal{X}_l) = \begin{cases} 1, & \mathcal{X}_l \geq L_t \\ \dfrac{\mathcal{X}_l - L}{L_t - L}, & L \leq \mathcal{X}_l < L_t \\ 0, & \mathcal{X}_l < L \end{cases}$$

- Energy-saving: A total amount of energy $E_t = 5.4$ MJ is expected to be consumed, while the maximum amount of energy is $E = 6$ MJ.

$$\mathrm{DS}^1(\mathcal{X}_E) = \begin{cases} 1, & \mathcal{X}_E \leq E_t \\ \dfrac{E - \mathcal{X}_E}{E - E_t}, & E_t < \mathcal{X}_E \leq E \\ 0, & \mathcal{X}_E > E \end{cases}$$

- Accuracy: The accuracy of sensor measurements is targeted at $A_t = 90\%$, while the accuracy threshold is set as $A = 80\%$.

$$\mathrm{DS}^2(\mathcal{X}_\varphi) = \begin{cases} 1, & \mathcal{X}_\varphi \geq A_t \\ \dfrac{\mathcal{X}_\varphi - A}{A_t - A}, & A \leq \mathcal{X}_{\varphi_k} < A_t \\ 0, & \mathcal{X}_\varphi < A \end{cases}$$

Experiment Results

To demonstrate the generality of ACMP, we applied it to a UUV case described in (Shevtsov and Weyns 2016). The constraint satisfaction models in this scenario are $\mathrm{DS}^1(\mathcal{X}_l)$ (scanning distance), $\mathrm{DS}^2(\mathcal{X}_E)$ (energy consumption) and $\mathrm{DS}^2(\mathcal{X}_\varphi)$ (accuracy). There are trade-offs between these constraints, e.g., when sensors (e.g., sensor 1) with a higher quality of surveillance is chosen, more energy is consumed, resulting in less distance scanned.

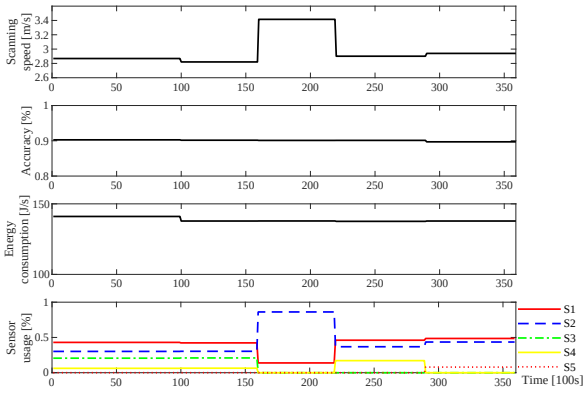

Figure 4: Adaptive-Constrained Motion Planning Results in the UUV Case.

Table 2: Constraints Satisfaction Results in the UUV Case.

QMs.	*Approaches*	# of disturbances				
		3	6	9	12	15
$\mathcal{X}_\varphi$ [%]	SCMP	88.9	87.5	85.8	84.4	82.4
	ACMP	***89.6***	***88.4***	***87.0***	***85.4***	***83.2***
$\mathcal{X}_l$ [km]	SCMP	99.9	99.2	98.0	96.6	94.5
	ACMP	***104.2***	***104.0***	***103.5***	***101.0***	***98.9***
$\mathcal{X}_E$ [MJ]	SCMP	5.34	5.33	5.31	5.34	5.34
	ACMP	***5.24***	***5.18***	***5.14***	***5.16***	***5.16***

[a] The violation tolerance are $\epsilon_\varphi = 10^{-3}$, $\epsilon_l = 0$, and $\epsilon_e = 0$.

Effectiveness The Fig. 4 shows the constraints-driven adaptation process of the UUV during operation with the case in (Shevtsov and Weyns 2016). At $k = 100$ we change the available energy change from 5.4 to 5.0 MJ, at $k = 160$ we change the distance to be scanned from 100 to 105 km. The plots show that these changes in constraints lead to corresponding changes in the arrangement of sensor usage, as the time portion for $S2$ increases. Figure 4 also shows how ACMP reacts to changes in sensor parameters and sensor failures. At $k = 220$, the measurement accuracy of sensor $S3$ drastically decreases from 83% to 43%, at $k = 290$, $S4$ stops working, and leads to an optimal solution that $S1$ is more exploited. At last, the mission end with average measurement accuracy at 90.1%, scanning distance at 106.7 km, energy consumption at 4.98 MJ.

Robustness In this scenario, the performance of the three methods are compared while adding random failures to parameters of sensors, i.e., sensor accuracy, scanning speed and energy consumption. For each method, we simulated

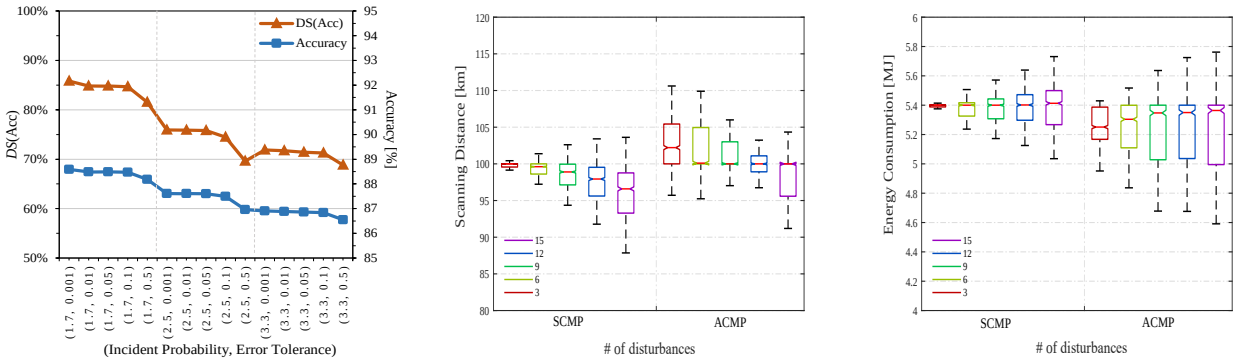

(a) Scanning accuracy with various disturbances and ϵ. (ACMP)

(b) Variance of scanning distance.

(c) Variance of energy consumption.

Figure 5: Scanning accuracy, distance and energy consumption with various probability of disturbances and violation tolerance.

UUV motion by adding different frequencies of random disturbances at different time instants. For each frequency of disturbances, we simulated 500 rounds and computed the average accuracy, scanning distance and energy consumption. The results are shown in Table 2. We can see that under ACMP, the UUV can scan a longer distance with higher accuracy and less energy consumption than SCMP. Moreover, the motion generated by SCMP can hardly satisfy all the three constraints, while the motion from ACMP can satisfy the timeliness and energy constraints, only slightly violating the accuracy constraint. The reason behind this is that at the *Constraints Satisfaction Analysis* stage, the accuracy is selected as the constraint for adaptation while the other two remain as their original soft goals as constraints. The variance of scanning distance and energy consumption of two strategies are compared in Figure 5(b) and Figure 5(c).

Table 3: Statistics on Overhead Data.

Cases	***Approaches***	***Average*** [s]	***Standard Deviation*** [s]
UAV	SCMP	0.2115	0.0879
	ACMP	***0.0811***	***0.0821***
UUV	SCMP	0.0423	0.0092
	ACMP	***0.0344***	***0.0217***

Real-time Performance Finally, we analyze the computation overhead of ACMP in generating an optimal self-adaptive plan. Table 3 shows the empirical distribution of the computation time for 10000 executions of each method in either simulation, where the red dotted lines represent the average computation time. From Table 3, the difference in average computation time between SCMP and ACMP is about 7 ms (0.0423 s versus 0.0344 s) in the UUV case, and 130 ms (0.2115 s versus 0.0811 s) in the UAV case.

This is because SCMP considers the optimization of all constraints while ACMP only considers the optimization of unsatisfied constraints, as constraints predicted to be satisfied are constraints. So SCMP requires more computation especially when there are more constraints to be considered. ACMP has larger variance since the number of constraints to be optimized may vary at runtime. In the worst case, when all the constraints need to be adjusted, the computation time of ACMP will be larger than SCMP. This is very rare from our experiment results. Hence, ACMP is flexible and capable of accommodating multiple constraints at runtime.

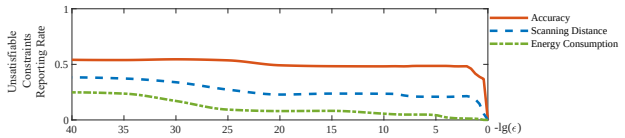

Figure 6: Unsatisfiable constraints reporting rate. (UUV case, # of disturbances = 9)

Choice of violation tolerance As discussed in the paper, the choice violation tolerance ϵ determine which constraint needs relaxation, while the larger the value is, the less number of constraints in the *Unsatisfied* constraint set, along with the underlying higher risk of no feasible solution. Thus the value of ϵ should be determined based on experimental data. The choice of different violation tolerance ϵ and the performance scanning accuracy achievement are illustrated in Figure 5(a). As the number of disturbances increases, the impact of ϵ on constraint satisfaction is more obvious. Figure 6 illustrates adaptation rate of each soft constraints in UUV case, as the increase of violation tolerance. In the UUV case, we choose $\epsilon_{\varphi,e,l} = \{10^{-3}, 0, 0\}$, when the adaptation rate of each constraint tends to be gentle.

References

Burian, S. J.; Velugubantla, S. P.; Chittineni, K.; Maddula, S. R. K.; and Brown, M. J. 2002. Morphological analyses using 3D building databases: Portland, Oregon. Technical report, Utah. LA-UR, Los Alamos National Laboratory, Los Alamos, NM.

Hidalgo-Panagua, A.; Vega-Rodríguez, M. A.; Ferruz, J.; and Pavón, N. 2017. Solving the multi-objective path plan-

ning problem in mobile robotics with a firefly-based approach. *Soft Computing* 21(4): 949–964.

Luo, Y.; Yu, Y.; Jin, Z.; Li, Y.; Ding, Z.; Zhou, Y.; and Liu, Y. 2020. Privacy-Aware UAV Flights through Self-Configuring Motion Planning .

Shevtsov, S.; and Weyns, D. 2016. Keep it simplex: Satisfying multiple goals with guarantees in control-based self-adaptive systems. In *Proceedings of the 2016 24th ACM SIGSOFT International Symposium on Foundations of Software Engineering*, 229–241. ACM.

Shevtsov, S.; Weyns, D.; and Maggio, M. 2019. SimCA*: A control-theoretic approach to handle uncertainty in self-adaptive systems with guarantees. *ACM Transactions on Autonomous and Adaptive Systems (TAAS)* 13(4): 17.